Rare Metal Materials and Engineering
Volume 52, Issue 5, May 2023
Available online at www.rmme.ac.cn

Science Press

Cite this article as: Qiang Meng, Yang Xirong, Liu Xiaoyan, et al. Progress of Ultrafine-Grain Ti and Its Alloys Prepared by ECAP for Biomedical Applications[J]. Rare Metal Materials and Engineering, 2023, 52(05): 1673-1682.

REVIEW

Progress of Ultrafine-Grain Ti and Its Alloys Prepared by ECAP for Biomedical Applications

Qiang Meng, Yang Xirong, Liu Xiaoyan, Luo Lei

College of Metallurgical Engineering, Xi'an University of Architecture and Technology, Xi'an 710055, China

Abstract: Ti and its alloys have become one of the most widely used biomedical metal materials due to their lightweight, low elastic modulus, excellent biocompatibility, and superb osseointegration. However, their low plasticity, inferior corrosion resistance, and poor wear resistance restrict the development and applications of Ti and its alloys. Severe plastic deformation is considered as one of the most effective methods for grain refinement of metal materials. Additionally, equal channel angular pressing (ECAP) is the commonly used preparation method for bulk ultrafine-grain (UFG)/nanocrystalline metal materials. Through ECAP deformation, UFG Ti and its alloys with superior comprehensive properties can be prepared. In this research, the progress of ECAP preparation for biomedical UFG Ti and its alloys was reviewed. The effects of ECAP deformation on the microstructure, mechanical properties, corrosion resistance, and wear resistance of Ti and its alloys were discussed. The deformation and grain refinement mechanisms were analyzed. The development direction of further optimization in the properties of Ti and its alloys through ECAP coupled with traditional plastic working methods and post-deformation heat treatment was proposed.

Key words: Ti alloys; ECAP; UFG; corrosion resistance; wear resistance

Biomedical materials can be used in human body as intravascular stents, cardiac simulator, and replacement implants for hips, knees, shoulders, and dentistry[1–2]. The implants have experienced rapid development in recent years[3]. Generally, the invalid implants are mainly caused by the mismatch in elastic modulus between the bones and implants, low strength, the generation of debris, metal ion release, and rejection reaction of the human body[4]. The ideal implant material is required to have low elastic modulus (15–30 GPa), excellent mechanical strength (fatigue strength), excellent corrosion resistance, great wear resistance, non-toxic elements, and excellent biocompatibility matching with human bones[5–6]. Therefore, based on the abovementioned considerations, 316L stainless steel (18Cr-14Ni-2.5Mo, wt%), Co-Cr-based alloys, and Ti and its alloys are widely employed as metallic implant materials[7–10]. However, the elastic modulus of 316L low-stress steel and Co-Cr-based alloy is too high of about 210 and 240 GPa, respectively, which is much higher than that of the human bone and prone to stress shielding effect, resulting in the loosening of implants[11]. In addition, during long-term service, the release of Ni and Co elements in the alloy is cytotoxic[12–14]. Ti and its alloys are ideal materials for human implants due to their lightweight, elevated specific strength, low elastic modulus, favorable corrosion resistance, excellent biocompatibility, and superior osseointegration[15–17]. Three generations of Ti and its alloys have been developed as biomedical materials[18]. The first generation is the α-type Ti alloy, such as pure Ti and Ti-6Al-4V alloy. The application of commercially pure Ti as body implants is restricted due to the low microhardness and poor wear resistance of pure Ti[19]. Despite its high mechanical properties, the wear resistance of Ti-6Al-4V alloy is inferior. Meanwhile, the Al and V ions are cytotoxic[20]. However, Ti-6Al-4V alloy is still the most widely used surgical Ti alloy. The second generation Ti alloy is $\alpha+\beta$ type Ti alloys, such as Ti-5Al-2.5Fe and Ti-6Al-7Nb alloys, which have high elastic modulus and are prone to stress shielding effects. However, the Al ion has cytotoxicity[21–23]. Zr, Mo, Ta, Nb, and other alloying elements replace the Al element in the Ti-based alloys, thereby forming the third-generation β-type Ti alloys. Ti-Nb series, Ti-Zr series, Ti-Mo

Received date: November 02, 2022
Foundation item: National Natural Science Foundation of China (51474170)
Corresponding author: Yang Xirong, Ph. D., Professor, College of Metallurgical Engineering, Xi'an University of Architecture and Technology, Xi'an 710055, P. R. China, E-mail: yangxr@xauat.edu.cn

series, and Ti-Ta series alloys also attract much attention, which have higher strength, lower elastic modulus, and better biocompatibility, as ideal biomedical materials[24–34].

Ti and its alloys have high friction coefficient and inferior wear resistance, and the wear resistance normally has a positive relationship with the corrosion resistance of alloys. Therefore, the wear and corrosion usually jointly damage the materials. Compared with Co-Cr-based alloys and low-stress steels, Ti alloys have worse corrosion properties and frictional and wear properties. Wear debris can be found in the tissue adjacent to the implant, leading to adverse cellular responses and implant loosening[35–36]. Equal channel angular pressing (ECAP) is an "internal and external" material processing method to prepare bulk nanocrystalline/ultrafine-grain (UFG) materials through severe plastic deformation[37–38]. Through ECAP deformation, the strength, microhardness, corrosion resistance, and fatigue properties of metal materials can be effectively improved with maintaining the good plasticity[39–43]. Currently, ECAP deformation has been usually applied to prepare UFG Ti, Mg, Al, Cu, and their alloys[44–52].

In this research, the preparation progress of the UFG Ti and its alloys by ECAP deformation was reviewed. The effects of ECAP deformation on the microstructure, mechanical properties, corrosion properties, and wear properties of biomedical Ti and its alloys were summarized. The mechanisms of ECAP deformation and grain refinement for biomedical Ti and its alloys were discussed. The development prospects of biomedical Ti and its alloys were proposed.

1 Microstructure of ECAP Ti and Its Alloys

1.1 Microstructure characteristics

It is well known that ECAP deformation can efficiently refine the grain size of metallic materials to obtain bulk UFG materials. The microstructure and grain size distributions of Ti-6Al-7Nb alloy after ECAP deformation are shown in Fig. 1[22]. Generally, the grain becomes finer with increasing the deformation passes, and normally the most significant grain refinement effect can be observed during the first two passes. The grain refinement reaches saturation state after 6–8 passes of ECAP deformation. Gunderov et al[53] conducted ECAP deformation with different passes on commercially pure Ti at 200 °C. It is found that after 6 passes, the grain size is 174 nm, whereas after 8 passes, the grain size increases to 195 nm. During the ECAP deformation, the material is subjected to severe shear forces, and a lot of crystal defects, such as dislocations and twinning, are introduced into the microstructure. It is generally believed that both dislocation slip and twinning occur during ECAP deformation, and the dislocation slip results in the lath microstructure. However, the mechanisms of deformation and grain refinement are complex. Wang et al[54] found that during ECAP deformation of Ti-1300 alloy, the coordination of grain rotation, intragranular multi-system slip, and dislocation-staggered arrangement at the grain boundary occurs, resulting in the unbroken grain boundary.

As a novel biomedical material with high strength and low elastic modulus, the microstructure evolution characteristics and deformation mechanism of β-Ti alloys during ECAP deformation attract much attention[55]. Li et al[56] performed ECAP deformation on Ti-36Nb-2Ta-3Zr alloy at room temperature. After ECAP process, the average grain size of β matrix and α'' martensite phase is significantly refined to 600 and 250 nm after 3 passes, and it is further reduced to 250 and 120 nm after 6 passes, respectively. The dominant deformation

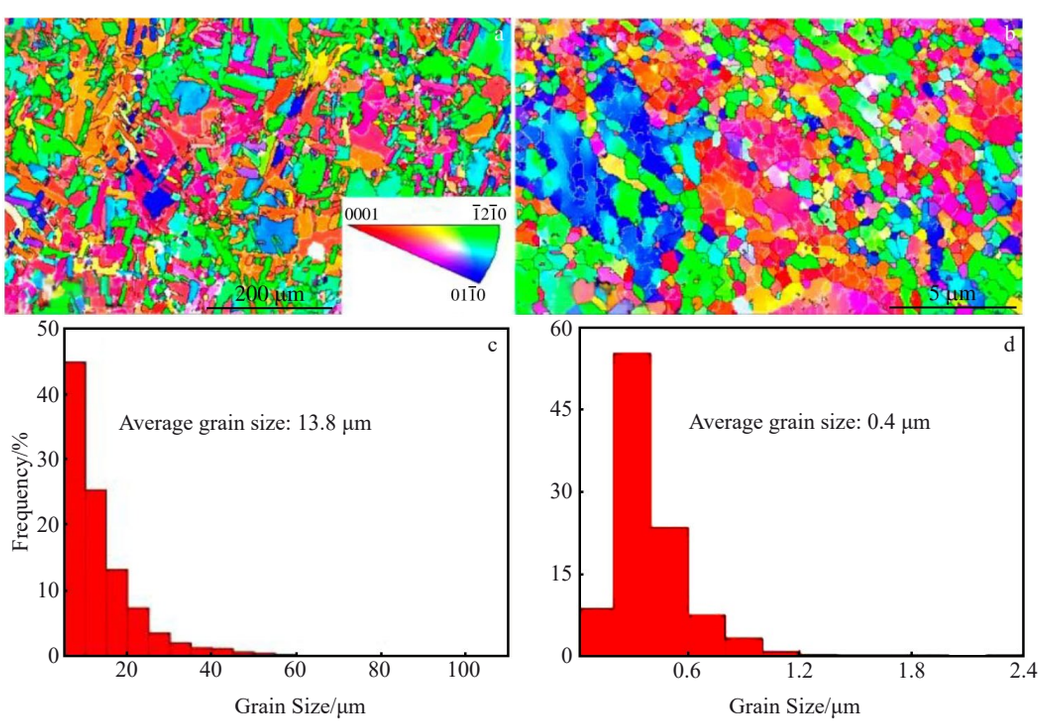

Fig.1 Microstructure (a–b) and grain size distributions (c–d) of coarse grains (a, c) and fine grains (b, d) in Ti-6Al-7Nb alloy[22]

mechanism of the coarse-grained Ti-36Nb-2Ta-3Zr alloy during ECAP process at room temperature involves the stress-induced martensitic transformation and dislocation activity. Lin et al[57] obtained the Ti-35Nb-3Zr-2Ta alloy with ultrafine equiaxed grains after ECAP deformation of 4 passes. Shear bands with intersecting networks and the twinned martensitic variants of herringbone microstructure can be observed after ECAP deformation process. Suresh et al[58] found that the grain refinement mechanism of Ti-13Nb-13Zr alloy is the local lattice rotation and dynamic recrystallization during ECAP deformation.

The proposed grain refinement mechanisms in ECAP deformation, including the dislocation structure evolution, shear band refinement, dynamic recrystallization refinement, and twin refinement, cannot lead to some specific microstructure features in the deformation process. Recently, the continuous dynamic recrystallization and grain subdivision mechanisms have been proposed. It is proved that the continuous dynamic recrystallization occurs in Ti alloys during ECAP deformation[59]. The mechanism of continuous dynamical recrystallization suggests that during the early stages of ECAP deformation, a lot of dislocations pile up at the original large angle grain boundaries, forming dislocated disentangled zones and lath structures. With increasing the strain, the dislocation density is increased, and the disentangled regions of the lath and dislocations evolve into dislocation cells, which continuously absorb the nearby dislocations. When the density of dislocation cell wall reaches a critical value, a large number of dislocations with different orientations are offset by each other, resulting in the gradually clear cell wall which further evolves into the sub-crystal. Then, the continuous dynamic recrystallization occurs, and the sub-grain is gradually transformed into equiaxed UFG microstructure with large angle grain boundaries[60]. The formation of UFG structure by ECAP can be explained by the grain subdivision mechanism, as shown in Fig. 2[61]. During ECAP deformation, multiple slip systems are activated due to the constraints of adjacent grains. The activation of different slip systems in different grain regions leads to different local crystal rotations, which results in the evolution of misorientation between adjacent regions and the geometrically necessary boundaries (GNBs). Numerous dislocations are also stored in the regions divided by GNBs, and the low-energy configurations, namely incidental dislocation boundaries (IDBs), are gradually formed. With increasing the strain, the original grains are subdivided by GNBs and IDBs, and finally the UFG structure is formed[62].

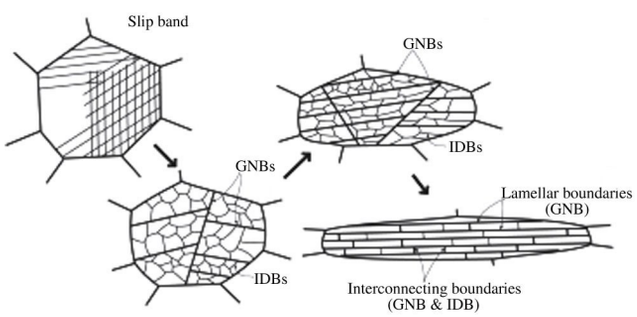

Fig.2 Schematic diagram of grain subdivision mechanism during ECAP deformation[61]

Ti has hexagonal close-packed (hcp) crystal structure and a few independent slip systems, which restricts its plastic deformation. However, the commercially pure Ti still exhibits good plasticity at room temperature due to the activation of twinning during plastic deformation. The main deformation twinning in pure Ti during ECAP deformation at room temperature includes $\{10\bar{1}2\}$ tensile twin, $\{11\bar{2}1\}$ tensile twin, and $\{11\bar{2}2\}$ compression twin. Generally, the activation of $\{10\bar{1}1\}$ twins requires high temperature and pressure[63–65]. However, it is found that $\{10\bar{1}1\}$ twins can be activated in pure Ti at room temperature. This is due to the severe shear force and large strain rate during ECAP deformation[66]. Temperature, strain rate, texture, and chemical composition all have significant effects on deformation twins. Also, the twins are highly sensitive to the grain size. The larger the grain size, the easier the activation of twins[67]. The deformation mechanism of UFG materials prepared by ECAP deformation also includes the grain boundary slip[68]. When the grain size is refined to the ultrafine or nanocrystalline scale, the grain size has a significant influence on the deformation mechanism. Zhu et al[69] studied the effect of grain size on the deformation mechanism. When the grain size is larger than 100 nm, the deformation mechanism is the dislocation slip. When the grain size is about 50 nm, the deformation mechanism is mainly dominated by the generation and annihilation of dislocations at the grain boundaries. When the grain size reduces to 10–50 nm, the deformation mechanisms are dislocation and twin coordination deformation. When the grain size is less than 10 nm, the deformation mechanism is dominated by grain boundary slip. Generally, the grain boundary slip only occurs at high temperatures. However, during severe plastic deformation, grain boundary slip can also occur at relatively low temperatures or even at room temperature.

1.2 Influence factors

ECAP deformation parameters, such as deformation temperature, route, pass, die angle, die size, extrusion speed, back pressure, and lubricant, can affect the morphology and homogeneity of the microstructure and mechanical properties of deformed materials. It is demonstrated that the angle between the channels, the outer angle, and the friction coefficient also have great influence on the strain homogeneity and the quality of the ECAP deformed materials[70–71]. Jiang et al[72] used Deform-3D software to simulate the effect of different influence factors on Ti-6Al-4V alloy during ECAP process. It is shown that the effect of equivalent stress and flow velocity on deformed alloy is more obvious than that of friction coefficient and temperature. Additionally, the extrusion force and the magnitude and distribution of equivalent strain are extremely sensitive to the friction coefficient.

1.2.1 Effect of deformation temperature

The higher the deformation temperature, the easier the

recovery during ECAP deformation, and the easier the grain growth, thereby degrading the refining effect[73]. However, ECAP deformation is particularly difficult for Ti with hcp structure at room temperature. Increasing the deformation temperature can effectively increase the processability of Ti. Therefore, a large number of researches focus on the ECAP deformation of Ti and its alloy at high temperatures. Semiatin et al[74] found that when the temperature increases to 275 °C or above, the alloy has smooth surface and no cracks can be observed. Zhao et al[75–76] successfully achieved ECAP deformation of commercially pure Ti at room temperature. Hu et al[77] used DEFORM software to simulate the ECAP process of pure iron-clad TA15 Ti alloy at room temperature. Based on the simulation analysis, the room temperature ECAP deformation of TA15 Ti alloy was successfully completed. Shahmir et al[78] achieved ECAP deformation of Ni-50.2at% Ti alloy at room temperature through core-sheath configuration. The ECAP deformation of 59Ti-36Nb-2Ta-3Zr Ti alloy can also be conducted at room temperature[78]. However, some Ti alloys cannot achieve ECAP deformation at room temperature due to their high strength, high microhardness, poor machinability, and insufficient lubrication. Besides, the low bearing capacity of hydraulic press also restricts the ECAP deformation at room temperature.

1.2.2 Effect of deformation route

The schematic diagram of typical ECAP deformation routes is shown in Fig.3, including route A, route B_A, route B_C, and route C[79]. The shear strain paths resulting from different deformation routes are shown in Fig.4[79]. It can be seen that the grain refinement can be achieved by multi-pass deformations with different routes, and the grain refinement through route B_C is the most effective. Route B_A has the worst refinement effect due to the strain offset phenomenon in the deformation process of adjacent passes[80]. Suh et al[81] believed that the material has the best elongation after deformation by route C, and presents the isotropic hardening behavior after deformation by route B_C. Therefore, route B_C and route C are commonly used ECAP route.

1.2.3 Effect of deformation passes and die angle

The cumulative equivalent strain calculation in ECAP deformation can be expressed by Eq.(1), as follows:

$$\varepsilon_N = \frac{N}{\sqrt{3}}\left[2\cot\left(\frac{\varphi}{2}+\frac{\psi}{2}\right)+\psi\csc\left(\frac{\varphi}{2}+\frac{\psi}{2}\right)\right] \quad (1)$$

where N is the number of ECAP passes, φ is the angle between channels, and Ψ is the outer angle. Thus, with increasing the deformation passes, the equivalent strain is increased, and the deformation is more severe. It is known

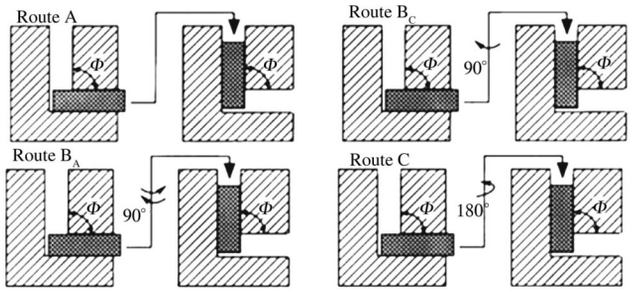

Fig.3 Schematic diagram of different ECAP deformation routes[79]

that the grain is gradually refined with increasing the number of ECAP deformation passes. The first 2 passes have the best refinement effect, and the grain refinement reaches saturation after deformation for 6–8 passes. With further increasing the deformation passes, the grain refinement effect is less obvious, but the microstructure homogeneity is increased. This is because the misorientation between the grains increases and the small angle grain boundaries change to the large angle grain boundaries.

The angle between channels (Φ) is the most significant factor affecting the strain and grain refinement effect[82]. It is easy to obtain refined and uniform equiaxed grains after deformation with Φ=90°. When Φ<90°, the deformation is more severe, but the alloy easily breaks due to deformation hardening during ECAP deformation. When Φ>90°, the single-pass deformation strain is slight, but the alloy can be repeatedly extruded to achieve the ideal grain refinement effect[83].

1.2.4 Effect of lubrication

ECAP deformation strongly depends on the friction coefficient. Reducing the friction coefficient can improve the microstructure uniformity and surface quality, reduce the extrusion force, and thus achieve better ECAP deformation of the alloy[84]. Hasani-Najafabadi et al[85] analyzed the lubrication effects of graphite, molybdenum disulfide, and zinc stearate on ECAP deformation of AL2024 alloy. It is found that the zinc stearate has better effects than other lubricants in ECAP process.

In addition, the extrusion speed, back pressure, die size, and other factors can also affect the deformation microstructure and properties of ECAP deformed materials[86–88]. The modern ECAP equipment and die can also be ameliorated to expand the application of ECAP technology[89–91].

2 Effect of ECAP Deformation on Properties of Ti and Its Alloys

After ECAP deformation, the grains of Ti and its alloy are refined, a large number of defects appear in the

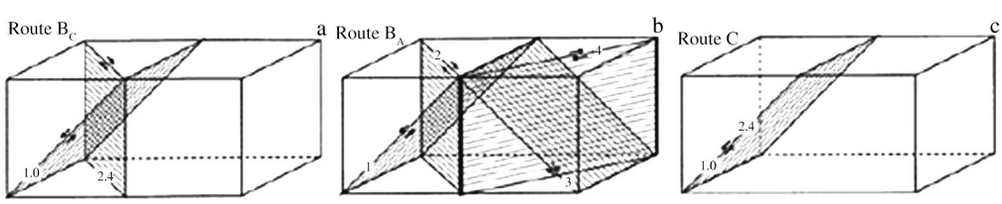

Fig.4 Shear strain paths for route B_C (a), route B_A (b), and route C (c) for 90° die of ECAP deformation[79]

microstructure, the preferred orientation is formed, and the stress concentration is relatively large. As a result, the strength and hardness of the material increase, the plasticity decreases, and the resistance against corrosion, wear, fatigue, and creep is improved. The property variation of Ti and its alloys after ECAP deformation is summarized in Table 1.

2.1 Mechanical properties

The UFG materials prepared by ECAP contain a large number of non-equilibrium large angle grain boundaries, which exhibit some properties different from those of conventional coarse grain materials, such as higher strength, higher microhardness, and lower strain hardening capability. Numerous studies have shown that the strength of Ti and its alloys can be effectively enhanced after ECAP deformation, while the plasticity is within acceptable limits. In addition, Ti is a metal with high melting temperature, and its microhardness is normally increased with increasing the ECAP deformation passes until it is saturated under a large strain[92]. However, when the ECAP deformation increases, the strength of the material approaches the saturation state. There also have been numerous attempts to enhance the uniform ductility of UFG Ti and its alloys or even to achieve room temperature super-plasticity[107–109]. Kuramoto et al[110] found that the optimal combination of ultra-high strength and high ductility can be achieved through lattice softening effect. The mechanical properties of ECAP-deformed Ti and its alloys are summarized in Table 2.

Grain refinement strengthening is one of the important strengthening mechanisms of metal materials[98]. The grain refinement behavior of ECAP-deformed Ti and its alloys is mainly caused by the combination effect of mechanical shear strength and dynamic recrystallization. It can be seen from the typical Hall-Petch relationship that the strength of metallic material can be significantly increased with decreasing the grain size. However, when the grain size is smaller than a certain critical value, the inverse Hall-Petch relationship occurs due to the transition of the deformation modes. Zheng et al[99] treated the pure Mg by severe plastic deformation followed by annealing to obtain the fully recrystallized UFG alloys. The grain size depends on the yield stress and total elongation of pure Mg with different average grain sizes, and their relationship is shown in Fig.5. The yield stress obeys the typical Hall-Petch relationship in the Region I (coarse-grained region), then is negatively deviated in the Region II (fine-grained region), and eventually exhibits the inverse Hall-Petch relationship in the Region III (UFG region).

By characterizing the microstructure of ECAP-deformed materials, the influence of dislocation and grain boundary on the yield strength of materials can be quantified. The yield strength can be expressed by Eq.(2), as follows:

$$\sigma=\sigma_0+\sigma_{gb}+\sigma_d \quad (2)$$

where σ_0 is the strengthening effect of friction stress, σ_{gb} is the grain boundary strengthening, σ_d is the dislocation strengthening. The grain boundary strengthening σ_{gb} can be expressed by Eq.(3)[112], as follows:

$$\sigma_{gb}=\sigma_{LABs}+\sigma_{HABs}=(MaG\sqrt{3|\boldsymbol{b}|\theta_{LAB}(1-f)}+k_{HP}\sqrt{F})D_b^{-1/2} \quad (3)$$

where σ_{LABs} and σ_{HABs} are the strengthening contributions of low-angle boundaries (LABs) and high-angle boundaries (HABs), respectively; M is the Taylor factor; a is a constant of the order of 0.1–0.5; G is the shear modulus; $\boldsymbol{b}$ is the Burgers vector; θ_{LAB} is the mean LAB misorientation; f is the HAB fraction; k_{HP} is Hall-Petch constant; D_b is the mean equivalent fragment diameter. The dislocation strengthening σ_d can be expressed be Eq.(4), as follows:

$$\sigma_d = MaG|\boldsymbol{b}|\rho^{0.5} \quad (4)$$

where ρ is the density of free dislocations. Dyakonov et al[113] deformed the pure Ti (grade 4) by ECAP at 200 °C for 12 passes. It is calculated that σ_{LABs}, σ_{HABs}, and σ_d is 406, 167, and 119 MPa, respectively. The calculated yield stress is 1117

Table 1 Property variation of Ti and its alloys after ECAP deformation

Property	Variation trend	Ref.
Strength	Increasing	[79,92–99]
Microhardness	Increasing	[78,92–94,97–98]
Plasticity	Decreasing	[92–99]
Corrosion	Increasing	[100–103]
	Decreasing	[104]
Wear	Increasing	[105–106]
	No change	[102]

Table 2 Summary of mechanical properties of ECAP deformed Ti and its alloys

Ti and its alloys	ECAP parameter	Ultimate tensile strength/MPa	Hardness, HV/×9.8 MPa	Elongation/%	Ref.
TA1	Room temperature, 120°, B_C, 8 passes	791	264	19	[111]
TA1	Room temperature, 90°, C, 4 passes	630	228	17.6	[112]
TA2	450 °C, 90°, B_C, 8 passes	710	272	14	[113]
TA4	450 °C, 90°, B_C, 4 passes	1240	-	1.6	[114]
Ti-6Al-4V	650 °C, 120°, B_C, 8 passes	1039	-	10	[115]
Ti-6Al-4V	450 °C, 120°, B_C, 4 passes	1432	392	-	[116]
Ti-35Nb-3Zr-2Ta	500 °C, 90°, B_C, 4 passes	765	216	16	[117]
Ti-6Al-7Nb	600 °C, 120°, B_C, 6 passes	1210	-	12	[118]
Ni-50.2Ti	Room temperature, 90°, C, 4 passes	-	214–304	-	[78]
Ti-36Nb-2Ta-3Zr	Room temperature, 120°, B_C, 6 passes	753.7	-	19.1	[56]

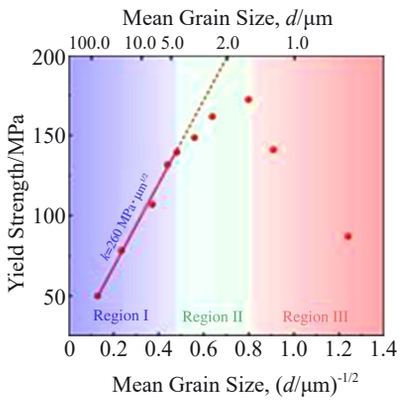

Fig.5 Relationship between yield stress and grain size[99]

MPa, while the measured yield stress is 1045 MPa. The difference between the calculated and the measured yield stress is very small, suggesting that the enhancement effect of ECAP is mainly related to the grain refinement, and the contribution of substructure to the enhancement effect cannot be neglected.

In addition, the studies on tensile and compressive deformation behavior of UFG pure Ti mainly focus on the properties of true stress-true strain curve, deformation, fracture properties, strain rate sensitivity to flow stress, and strain hardening index. Alexandrov et al[114] found that the strain hardening of UFG pure Ti is decreased with the ECAP process proceeding. Jia et al[115] found that the strain rate sensitivity index of UFG pure Ti is significantly lower than that of chemically pure (CP) Ti, indicating that the uniform plastic deformation ability and work hardening ability of UFG pure Ti are inferior.

2.2 Corrosion properties

The corrosion properties of metallic materials are mostly investigated through electrochemical potentiodynamic polarization experiments, or mass loss experiment by immersion tests. The corrosion kinetics is related to the corrosion mode, and the corrosion mechanism is related to the material microstructure. The corrosion properties of UFG Ti and its alloys are still unclear. Generally, the passivity of UFG Ti obeys the Ralston rule, and the corrosion resistance is improved after ECAP deformation[116]. Balakrishnan et al[117] conducted 4 passes of ECAP deformation on CP Ti (grade 2) at 350 °C, and compared the corrosion properties of CP Ti and UFG Ti in simulated body fluid. The results show that the corrosion resistance of UFG Ti is 10 times higher than that of CP Ti due to the faster surface passivation and stronger oxide film under the influence of dislocation and residual compressive stress. Balyanov et al[118] compared the electrochemical corrosion properties of CP Ti and UFG Ti prepared by ECAP in HCl and H_2SO_4 solutions of different concentrations, and pointed out that UFG Ti has lower corrosion current density and slower corrosion rate than CP Ti does. Suresh et al[58,100] conducted 8 passes of ECAP deformation on Ti-13Nb-13Zr alloys at 600 °C with the die angle of 120° through route B_C. It is found that the corrosion properties of Ti-13Nb-13Zr alloy deformed by ECAP are greatly improved. Although ECAP deformation can improve the corrosion resistance of Ti and its alloys, several contradictory results[101] are also reported.

The corrosion properties of materials can be affected by grain size, grain size distribution, passivation properties, texture, segregation of alloying elements, residual stress, and corrosive medium[102–104]. Miyamoto et al[101] believed that the relationship between corrosion resistance and grain size is decided by the degree of local corrosion, rather than the active or passive state. Qin et al[119] found that grain refinement can improve the stress corrosion resistance by increasing the number of grain boundaries. Hashemi et al[120] reported that the corrosion resistance of ECAP-deformed pure Ti is enhanced, which is related to the influence of grain refinement on the formation of passive film. Gollapudi et al[121] found that the grain size determines the thickness, density, and element distribution of the passive film, and the grain size distribution significantly affects the uniformity of the passive film, thereby affecting the electrochemical corrosion performance of the material. For UFG materials with the similar average grain size, the wider the grain size distribution, the worse the corrosion resistance[122].

Miyamoto et al[123] reported that the introduction of high-density lattice defects during ECAP process can enhance the corrosion kinetics. Hoseini et al[124] found that the presence of texture significantly improves the corrosion resistance of UFG Ti. Different types of texture have different effects on polarization resistance and corrosion current density, and the basal texture of UFG Ti can exert the optimal corrosion resistance[124–125]. Moreover, Kim et al[126] showed that the gradually enhanced basal texture and the continuously refined grain size jointly promote the corrosion resistance of UFG Ti. As for the influence of corrosive medium, it is found that the corrosion resistance of UFG materials is better than that of coarse-grained materials in passive environments[127].

In conclusion, after ECAP deformation, the significant grain size refinement, texture formation, a large number of defects, and stress concentration can all be observed in the deformed alloy. On the one hand, the grain refinement leads to the high-density grain boundaries in the microstructure, which reduces the segregation of impurity atoms at the grain boundaries, thereby resulting in the more uniform electrochemical properties of the material surface and reducing the grain boundary corrosion. Additionally, the grain boundary energy is higher, which can increase the surface reactivity by exciting the electronic activity and diffusion, thus improving the adhesion of passivation layer. On the other hand, the passive film is generated at the lattice defects, and ECAP deformation introduces high-density dislocations and residual stress, which improves the formation rate of passive film. Therefore, ECAP deformation improves the corrosion resistance of the Ti and its alloys.

2.3 Wear properties

The common wear performance test is the contact reciprocating wear test, as shown in Fig. 6[36]. The wear properties can be quantitatively characterized by calculating

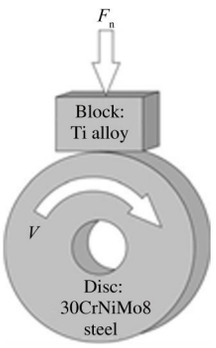

Fig.6 Schematic diagram of wear test[36]

the friction coefficient. The wear mechanism of metal materials includes the adhesive wear, abrasive wear, fatigue wear, corrosive wear, oxidation wear, and delamination wear. Ti alloys have inferior friction and wear properties due to their low work hardening rate, inferior plastic shear resistance, and low surface hardness[128]. The wear properties of Ti and its alloys are affected by the synergistic effects of load, sliding speed, temperature, wear materials, and friction medium. Generally, the greater the load, the smaller the sliding speed, the lower the temperature. Besides, the greater the hardness of abrasive material, the greater the wear rate of material.

ECAP can effectively improve the mechanical strength and wear resistance, which has been widely used for Al alloys, Mg alloys, Cu alloys, and steels[129–132]. Moreover, ECAP deformation route may affect the wear properties[133]. Currently, the effect of ECAP on the wear properties of Ti and its alloys is rarely reported. The comparative study on the wear properties of CP Ti and UFG Ti shows that the UFG microstructure leads to the lower adhesive composition, which reduces the friction coefficient and improves the wear properties[134]. Zhang et al[135] investigated the effect of ECAP deformation on oxide layer formation and wear properties of pure Ti surfaces. The results show that ECAP process can promote the formation of oxide layer on Ti surface and improve the microhardness and wear resistance of oxide layer. Repeated loading due to reciprocal friction induces the permanent plastic deformation on the material surface, which leads to the dislocation slip in the internal microstructure. The dislocation slip is blocked at the grain boundaries, forming a plug which gradually results in the large stress concentration. When the stress exceeds the yield limit of material, microcracks are initiated and then expanded with increasing the wear depth, eventually leading to the formation of worn debris. The fine grain strengthening of ECAP-deformed materials results in the increase in yield stress, which increases the critical stress of dislocation slip, enhances the deformation resistance, delays the occurrence of plastic deformation and cracks, and finally improves the wear resistance[136]. It is reported that the higher hardness and lower ductility can effectively reduce the adhesive wear of materials. In conclusion, ECAP deformation can improve the wear resistance of Ti and its alloys.

Generally, the higher the microhardness, the lower the wear rate during the abrasive wear. However, Stolyarov et al[137] found that there is no notable difference in the wear resistance under different microstructures and microhardness. Therefore, the influence mechanisms of wear properties are still obscure, which should be further studied.

3 Restrictions and Development

Although ECAP shows great application potential, several restrictions of ECAP deformation still exist. (1) ECAP deformation has refinement limit and strengthening limit due to the dislocation recovery. Normally, after deformation for 6–8 passes, the material strength is decreased with increasing the deformation passes[138]. (2) The shape and size of the die restrict the product size in practical application. Combining ECAP with traditional plastic processing can solve the problem of strengthening limit and improve the material properties. Stolyarov et al[137] combined ECAP (8 passes) with cold rolling to prepare UFG CP Ti with the yield stress of 1000 MPa. Semenova et al[138] combined ECAP (8 passes) with forging and drawing to prepare CP Ti, and the yield stress of UFG CP Ti also reached 1000 MPa. Polyakov et al[139] combined ECAP (8 passes) with cold drawing to prepare UFG CP Ti, and its yield stress reached 1220 MPa. Therefore, the combined deformation method of ECAP with traditional plastic processing can solve the problems of strengthening limit and product size.

In addition, the post-deformation heat treatment process has been proposed, which can simultaneously improve the strength, plasticity, and even corrosion properties of the material[140–143]. Gu et al[42] performed rotary-die-ECAP deformation (4 passes) on CP Ti (grade 2) at 420 °C. After deformation, the alloys are subjected to annealing at 300 °C for 15, 30, and 60 min. The results show that after annealing, due to the enhancement of basal texture, the strength of the CP Ti is increased and the corrosion performance is improved. Semenova et al[94] conducted ECAP deformation of 4 passes+hot rolling+drawing on CP Ti (grade 4) at 450 °C with die of 90° and route B_C followed by annealing at 300–500 °C for 1 h. The results show that the grain size of deformed pure Ti is 150 nm, the ultimate tensile strength is 1240 MPa, and elongation is 1.6%. After annealing at 350 °C for 1 h, the ultimate tensile strength is 1320 MPa, and the elongation is 2.6%. After annealing at 350 °C for 6 h, the grain size is 170 nm, the ultimate tensile strength is 1450 MPa, and the elongation is 4.5%. The simultaneous enhancement in strength and ductility after annealing is caused by the recovery of the non-equilibrium grain boundaries, the rearrangement of the grain boundary structure, and the segregation of impurity atoms. Therefore, the appropriate thermal treatment of UFG Ti and its alloys can further improve the properties.

4 Conclusions

In recent years, β-type Ti alloys show great potential in biomedical applications due to their excellent properties. In this research, the microstructure, mechanical properties,

corrosion resistance, and wear resistance of ultrafine grain (UFG) biomedical Ti and its alloys prepared by equal channel angular pressing (ECAP) were reviewed. ECAP deformation and grain refinement mechanisms of Ti and its alloys were discussed. It is of theoretical and practical significance to improve the corrosion and wear properties of β-type Ti alloys for their potential performance in the biomedical field.

References

1 Geetha M, Singh A K, Asokamani R *et al*. *Progress in Materials Science*[J], 2009, 54(3): 397

2 Zhang L C, Klemm D, Eckert J *et al*. *Scripta Materialia*[J], 2011, 65(1): 21

3 Rehman M, Madni A, Webster T J. *Expert Review of Medical Devices*[J], 2018, 15(3): 193

4 Gepreel M A H, Niinomi M. *Journal of the Mechanical Behavior of Biomedical Materials*[J], 2013, 20: 407

5 Kurtz S M. *Journal of Bone & Joint Surgery*[J], 2007, 89(S3): 144

6 Bahl S, Suwas S, Chatterjee K. *International Materials Reviews*[J], 2021, 66(2): 114

7 Navarro M, Michiardi A, Castano O *et al*. *Journal of the Royal Society Interface*[J], 2008, 5(27): 1137

8 Prasad K, Bazaka O, Chua M *et al*. *Materials*[J], 2017, 10(8): 884

9 Zhang Y S, Wang X, Zhang W *et al*. *Materials Science and Engineering A*[J], 2017, 696: 360

10 Liu L H, Yang C, Wang F *et al*. *Materials & Design*[J], 2015, 79: 1

11 Guo L Y, Naghavi S A, Wang Z Q *et al*. *Materials & Design*[J], 2022, 216: 110 552

12 Li Y H, Yang C, Zhao H D *et al*. *Materials*[J], 2014, 7(3): 1709

13 Kuroda D, Niinomi M, Morinaga M *et al*. *Materials Science and Engineering A*[J], 1998, 243(1–2): 244

14 Okazaki Y, Gotoh E. *Biomaterials*[J], 2005, 26(1): 11

15 Zhang L C, Kim K B, Yu P *et al*. *Journal of Alloys & Compounds*[J], 2007, 428(1–2): 157

16 Calin M, Zhang L C, Eckert J. *Scripta Materialia*[J], 2007, 57(12): 1101

17 Planell J A, Navarro M. *Bone Repair Biomaterials*[M]. Cambridge: Woodhead Publishing, 2009: 3

18 Zhang L C, Chen L Y. *Advanced Engineering Materials*[J], 2019, 21(4): 1 801 215

19 Abbasi M, Ahmadi F, Farzin M. *Metals and Materials International*[J], 2021, 27(4): 705

20 Bordji K, Jouzeau J Y, Mainard D *et al*. *Biomaterials*[J], 1996, 17(9): 929

21 Avinash D, Kumar S P L. *Materials Technology*[J], 2022, 37(9): 897

22 Yu Z Q, Dong Y C, Li X *et al*. *Metals*[J], 2020, 10(7): 950

23 Avinash D, Kumar S P L. *Journal of Mechanical Science and Technology*[J], 2020, 34: 3757

24 Weng W J, Biesiekierski A, Li Y C *et al*. *Materialia*[J], 2019, 6: 100 323

25 Lee M K, Lee H, Kim H E *et al*. *Nanomaterials*[J], 2021, 11(6): 1507

26 Acharya S, Gupta P, Chatterjee K *et al*. *Materials Science Forum*[J], 2018, 941: 2465

27 Hu M C, Wang L, Li G *et al*. *Intermetallics*[J], 2022, 145: 107 568

28 Nunes A R V, Borborema S, Malet L *et al*. *Microscopy and Microanalysis*[J], 2019, 25(S2): 2634

29 Dsmva B, Jsa B, Yl B *et al*. *Materials Science and Engineering C*[J], 2019, 96: 466

30 Valkov S, Dechev D, Ivanov N *et al*. *Metals*[J], 2021, 11(8): 1246

31 Mareci D, Chelariu R, Gordin D M *et al*. *Acta Biomaterialia*[J], 2009, 5(9): 3625

32 Zhou Y L, Niinomi M, Akahori T *et al*. *Materials Science and Engineering A*[J], 2005, 398(1–2): 28

33 Kaur M, Singh K. *Materials Science and Engineering C*[J], 2019, 102: 844

34 Mohan P, Rajak D K, Pruncu C I *et al*. *Micron*[J], 2020, 142: 102 992

35 Simka W, Krząkała A, Masełbas M *et al*. *RSC Advances*[J], 2013, 3(28): 11 195

36 Cvijović-Alagić I, Cvijović Z, Mitrović S *et al*. *Tribology Letters*[J], 2010, 40: 59

37 Segal V M, Reznikov V I, Dobryshevshiy A E *et al*. *Russian Metallurgy* (*Metally*)[J], 1981(1): 99

38 Valiev R Z, Krasilnikov N A, Tsenev N K. *Materials Science and Engineering A*[J], 1991, 137: 35

39 Gunderov D V, Kim K A, Churakova A A *et al*. *Physics of Metals and Metallography*[J], 2022, 123(10): 1031

40 Gu Y X, Jiang J H, Ma A B *et al*. *Journal of Materials Research and Technology*[J], 2021, 15: 1873

41 Semenova I P, Polyakov A V, Polyakova V *et al*. *Materials Science and Engineering A*[J], 2017, 696: 166

42 Gu Y X, Ma A B, Jiang J H *et al*. *Materials Characterization*[J], 2018, 138: 38

43 Zhao Z Y, Wang G F, Zhang Y L *et al*. *Journal of Materials Engineering and Performance*[J], 2020, 29(2): 905

44 Koujalagi M B, Siddesha H S. *Materials Today: Proceedings*[J], 2020, 45: 71

45 Zhilyaev A P, Morozova A, Cabrera J M *et al*. *Journal of Materials Science*[J], 2016, 52: 305

46 Divya S P, Nagaraj M, Kesavamoorthy M *et al*. *Transactions of the Indian Institute of Metals*[J], 2018, 71: 67

47 Li G S, Fang M, Xu G S *et al*. *Materials Science and Technology*[J], 2022, 38(3): 181

48 Wei W, Wang S L, Wei K X *et al*. *Journal of Alloys & Compounds*[J], 2016, 678: 506

49 Wang G W, Song D, Zhou Z K *et al*. *Journal of Materials Research and Technology*[J], 2021, 15: 2419

50 Lei W W, Liang W, Wang H X *et al*. *Vacuum*[J], 2017, 144: 281

51 Tang L L, Zhao Y H, Islamgaliev R K *et al*. *Materials Science and Engineering A*[J], 2016, 670: 280

52 Lei W W, Zhang H. *Materials Letters*[J], 2020, 271: 127 781

53 Gunderov D V, Polyakov A V, Semenova I P *et al*. *Materials Science and Engineering A*[J], 2013, 562: 128

54 Wang Xinhan, Yang Xirong, Lu Jinwen *et al*. *Journal of Plasticity Engineering*[J], 2019, 26(5): 147 (in Chinese)

55 Mao C Y, Yu W J, Jin M *et al*. *Bioactive Materials*[J], 2022, 16: 15

56 Li Z M, Zheng B L, Wang Y T *et al*. *Journal of Materials Science*[J], 2014, 49(19): 6656

57 Lin Z J, Wang L Q, Xue X B *et al*. *Materials Science and Engineering C*[J], 2013, 33(8): 4551

58 Suresh K S, Gurao N P, Satyaveer S D *et al*. *Materials Characterization*[J], 2013, 82: 73

59 Zhang Yue. *Investigations on Microstructure and Mechanical Properties of Typical Metals After Severe Plastic Deformation*[D]. Nanjing: Nanjing University of Science and Technology, 2010 (in Chinese)

60 Liu Xiaoyan. *Study on Deformation Behavior and Microstructure and Mechanical Properties of Commercially Pure Ti Processed by ECAP at Room Temperature*[D]. Xi ' an: Xi ' an University of Architecture and Technology, 2014 (in Chinese)

61 Tsuji N, Gholizadeh R, Ueji R *et al*. *Materials Transactions*[J], 2019, 60(8): 1518

62 Hansen N, Mehl R F. *Metallurgical and Materials Transactions A*[J], 2001, 32(12): 2917

63 Tsuji N. *The Journal of the Iron & Steel Institute of Japan*[J], 2008, 94(12): 582

64 Chen Y J, Li Y J, Walmsley J C *et al*. *Scripta Materialia*[J], 2011, 64(9): 904

65 Minonishi Y, Morozumi S, Yoshinaga H. *Scripta Metallurgica*[J], 1985, 19(10): 1241

66 Qiang M, Yang X R, Liu X Y *et al*. *Rare Metal Materials and Engineering*[J], 2022, 51(6): 1949

67 Ghaderi A, Barnett M R. *Acta Materialia*[J], 2011, 59(20): 7824

68 Chinh N Q, Vörös G, Szommer P. *Materials Science Forum*[J], 2006, 503–504: 1001

69 Zhu Y T, Langdon T G. *Materials Science and Engineering A*[J], 2005, 409(1–2): 234

70 Djavanroodi F, Omranpour B, Ebrahimi M *et al*. *Progress in Natural Science: Materials International*[J], 2012, 22(5): 452

71 Dumoulin S, Roven H J, Werenskiold J C *et al*. *Materials Science and Engineering A*[J], 2005, 410: 248

72 Jiang Wenhuan. *Simulation Study on a Process of ECAP Deformation for Ti6Al4V Titanium Alloy*[D]. Chongqing: Chongqing University, 2020 (in Chinese)

73 Raab G I, Soshnikova E P, Valiev R Z. *Materials Science and Engineering A*[J], 2004, 387(389): 674

74 Semiatin S L, Delo D P. *Materials & Design*[J], 2000, 21(4): 311

75 Zhao X C, Fu W J, Yang X R *et al*. *Scripta Materialia*[J], 2008, 59(5): 542

76 Zhao X C, Yang X R, Liu X Y *et al*. *Materials Science and Engineering A*[J], 2010, 527(23): 6335

77 Hu Yulong, Liu Xiaoyan, Gao Feilong *et al*. *Journal of Plasticity Engineering*[J], 2022, 29(6): 39 (in Chinese)

78 Shahmir H, Nili-Ahmadabadi M, Mansouri-Arani M *et al*. *Advanced Engineering Materials*[J], 2015, 17(4): 532

79 Stolyarov V, Zhu Y T, Alexandrov I V *et al*. *Materials Science and Engineering A*[J], 2001, 299: 59

80 Iwahashi Y, Horita Z, Nemoto M *et al*. *Acta Materialia*[J], 1998, 46(9): 3317

81 Suh J, Victoria H J, Letzig D *et al*. *Materials Science and Engineering A*[J], 2016, 669: 159

82 Yang Xirong, Jing Feifei, Liu Xiaoyan *et al*. *Chinese Journal of Rare Metals*[J], 2018, 42(4): 367 (in Chinese)

83 Nakashima K, Horita Z, Nemoto M *et al*. *Acta Materialia*[J], 1998, 46(5): 1589

84 Xu Shubo. *Numerical Simulation and Experimental Investigation of Deformation Mechanism in Equal Channel Angular Pressing/Extrusion Process*[D]. Jinan: Shandong University, 2006 (in Chinese)

85 Hasani-Najafabadi S H, Neyestanak A L, Daneshmand S. *Industrial Lubrication and Tribology*[J], 2017, 69(5): 701

86 Li M Q, Zhang C, Luo J *et al*. *Rare Metals*[J], 2010, 29(6): 613

87 Zhao Z, Hou H, Zhang Y *et al*. *IOP Conference Series: Materials Science and Engineering*[J], 2018, 301(1): 12 077

88 Djavanroodi F, Ebrahimi M. *Materials Science and Engineering A*[J], 2010, 527(4–5): 1230

89 Mathieu J P, Suwas S, Eberhardt A *et al*. *Journal of Materials Processing Technology*[J], 2006, 173: 29

90 Fereshteh-Saniee F, Sepahi-Boroujeni A, Sepahi-Boroujeni S. *The International Journal of Advanced Manufacturing Technology*[J], 2016, 86(9): 3471

91 Torabi M, Eivani A R, Jafarian H *et al*. *Advanced Engineering Materials*[J], 2016, 18(8): 1469

92 Kawasaki M. *Journal of Materials Science*[J], 2014, 49: 18

93 Liu X Y, Zhao X C, Yang X R *et al*. *Advanced Engineering Materials*[J], 2014, 16(4): 371

94 Semenova I, Salimgareeva G, Da Costa G *et al*. *Advanced Engineering Materials*[J], 2010, 12(8): 803

95 Arabi H, Ketabchi M, Alhosseini S H N. *Rare Metals*[J], 2022, 41(8): 2732

96 Zhao Z Y, Wang G F, Zhang Y L *et al*. *Journal of Materials Engineering and Performance*[J], 2020, 29(2): 905

97 Polyakova V, Semenova I P, Polyakov A V *et al*. *Materials Letters*[J], 2017, 190: 256

98 Balasubramanian N, Langdon T G. *Metallurgical and Materials Transactions A*[J], 2016, 47(12): 5827

99 Zheng R, Du J P, Gao S *et al*. *Acta Materialia*[J], 2020, 198: 35

100 Suresh K S, Geetha M, Richard C *et al*. *Materials Science and Engineering C*[J], 2012, 32(4): 763

101 Miyamoto H. *Materials Transactions*[J], 2016, 57(5): 559

102 López M F, Gutiérrez A, Jiménez J A. *Surface Science*[J], 2001, 482: 300

103 López M F, Jiménez J A, Gutiérrez A. *Vacuum*[J], 2011, 85(12): 1076

104 Alateyah A I, Alawad M O, Aljohani T A *et al*. *Materials*[J], 2022, 15(16): 5515

105 Lee T, Mathew E, Rajaraman S *et al*. *International Journal of*

Nanomedicine[J], 2015, 10(S1): 207
106 Zhao X C, Yang X R, Liu X Y *et al*. *Materials Science and Engineering A*[J], 2010, 527(23): 6335
107 Kawasaki M, Langdon T G. *Reviews on Advanced Materials Science*[J], 2018, 54(1): 46
108 Langdon T G. *Solid State Phenomena*[C]. Zurich: Trans Tech Publications Ltd, 2020, 306: 1
109 Kawasaki M, Langdon T G. *Materials Transactions*[J], 2019, 60(7): 1123
110 Kuramoto S, Furuta T. *Materials Transactions*[J], 2019, 60(7): 1116
111 Yang Xirong, Zhao Xicheng, Wang Cheng *et al*. *Journal of Aeronautical Materials*[J], 2011, 31(1): 25 (in Chinese)
112 Hansen N. *Scripta Materialia*[J], 2004, 51(8): 801
113 Dyakonov G S, Mironov S, Semenova I P *et al*. *Materials Letters*[J], 2017, 192: 165
114 Alexandrov I, Chembarisova R, Sitdikov V *et al*. *Materials Science and Engineering A*[J], 2008, 493(1–2): 170
115 Jia D, Wang Y M, Ramesh K T *et al*. *Applied Physics Letters*[J], 2001, 79(5): 611
116 Ralston K D, Birbilis N. *Corrosion*[J], 2010, 66(7): 75 005
117 Balakrishnan A, Lee B C, Kim T N *et al*. *Trends in Biomaterials & Artificial Organs*[J], 2008, 22(1): 58
118 Balyanov A, Kutnyakova J, Amirkhanova N A *et al*. *Scripta Materialia*[J], 2004, 51(3): 225
119 Qin J, Li Z, Ma M Y *et al*. *Transactions of Nonferrous Metals Society of China*[J], 2022, 32(3): 765
120 Hashemi P M, Borhani E, Nourbakhsh M S. *Journal of Applied Biomaterials & Functional Materials*[J], 2022, 20: 22 808 000 221 095 234
121 Gollapudi S. *Corrosion Science*[J], 2012, 62(4): 90
122 Dobkowska A, Cielak B A, Kuc D *et al*. *Journal of Materials Research and Technology*[J], 2021, 13: 346
123 Miyamoto H, Harada K, Mimaki T *et al*. *Corrosion Science*[J], 2008, 50(5): 1215
124 Hoseini M, Shahryari A, Omanovic S *et al*. *Corrosion Science*[J], 2009, 51(12): 3064
125 Gurao N P, Manivasagam G, Govindaraj P *et al*. *Metallurgical and Materials Transactions A*[J], 2013, 44(12): 5602
126 Kim H S, Yoo S J, Ahn J W *et al*. *Materials Science and Engineering A*[J], 2011, 528(29–30): 8479
127 Wan X, Lan A, Zhang M *et al*. *Journal of Alloys and Compounds*[J], 2023, 944: 169 217
128 Yu Chengjun. *Modern Salt and Chemical Industry*[J], 2020, 47(3): 42 (in Chinese)
129 Gopi K R. *Materials Research Express*[J], 2020, 7(1): 16 550
130 Thiyaneshwaran N, Sureshkumar P. *International Journal of Engineering Research & Technology*[J], 2013, 2(5): 17
131 Gadallah E A, Ghanem M A, El-Hamid A M *et al*. *Am J Sci Technol*[J], 2014, 1: 60
132 Gao N, Wang C T, Wood R J K *et al*. *Journal of Materials Science*[J], 2012, 47(12): 4779
133 Yilmaz T A, Totik Y, Senoz G M L *et al*. *Materials Today Communications*[J], 2022, 33: 104 628
134 Stolyarov V, Shuster L S, Migranov M S *et al*. *Materials Science and Engineering A*[J], 2004, 371(1–2): 313
135 Zhang B S, Wang J Y, Zhu S S *et al*. *Oxidation of Metals*[J], 2019, 91: 483
136 Divya S P, Nagaraj M, Kesavamoorthy M *et al*. *Transactions of the Indian Institute of Metals*[J], 2018, 71(1): 67
137 Stolyarov V, Zeipper L, Mingler B *et al*. *Materials Science and Engineering A*[J], 2008, 476(1–2): 98
138 Semenova I P, Salimgareeva G K, Latysh V *et al*. *Materials Science and Engineering A*[J], 2009, 503(1–2): 92
139 Polyakov A V, Gunderov D V, Raab G I. *Materials Science Forum*[J], 2010, 667–669: 1165
140 Yuan Y C, Ma A B, Gou X F *et al*. *Materials Science and Engineering A*[J], 2015, 630: 45
141 Tao J M, Chen G M, Jian W W *et al*. *Materials Science and Engineering A*[J], 2015, 628: 207
142 Gubicza J, Pereira P H R, Kapoor G *et al*. *Advanced Engineering Materials*[J], 2018, 20: 1 800 184
143 Tian Y Z, Gao S, Zheng R X *et al*. *Journal of Materials Science and Technology*[J], 2020, 48: 31

ECAP制备超细晶生物医用钛及钛合金的研究进展

强　萌，杨西荣，刘晓燕，罗　雷
(西安建筑科技大学 冶金工程学院，陕西 西安 710055)

摘　要：钛及钛合金由于质轻、弹性模量低、生物相容性佳和骨整合性优异，已成为应用最广泛的生物医学金属材料之一。然而，较低的塑性、耐腐蚀性能和耐磨损性能限制了其发展和应用。剧烈塑性变形被认为是对金属材料最有效的晶粒细化方法之一，其中，等通道转角挤压（ECAP）是制备块状超细晶（UFG）/纳米晶金属材料的常用技术。通过ECAP变形，可以制备具有优异综合性能的UFG钛及钛合金。本文综述了生物医用UFG钛及钛合金的ECAP制备方式，着重讨论了ECAP变形对钛及钛合金的组织、力学性能、耐腐蚀性能和耐磨损性能的影响，分析了钛及钛合金的ECAP变形机制和晶粒细化机制，提出了通过ECAP变形结合传统塑性加工和变形后热处理来进一步优化钛及钛合金综合性能的想法。

关键词：钛合金；ECAP；UFG；耐腐蚀性能；耐磨损性能

作者简介：强　萌，女，1992年生，博士，西安建筑科技大学冶金工程学院，陕西 西安 710055，E-mail：1179566634@qq.com